# Channel Estimation for Joint Communication and Sensing in OFDM-FMCW Systems

Yeong Choi and Seongwook Lee

Department of Electrical and Electronics Engineering

College of ICT Engineering, Chung-Ang University

Seoul, Republic of Korea

{dodrmfl02, seongwooklee}@cau.ac.kr

Abstract—Joint communication and sensing (JCS) has emerged as a fundamental technology for sixth-generation wireless systems. The integration of orthogonal frequency-division multiplexing (OFDM) with frequency-modulated continuous waveforms (FMCW) presents a practical solution that preserves communication efficiency while enabling low-complexity sensing. However, a key challenge in this integrated waveform is the mutual interference between data symbols and chirp signals, which degrades both channel estimation accuracy and radar processing performance. Conventional superimposed-pilot (SP) estimation methods address this interference through multi-symbol averaging, but this approach becomes unreliable in fast time-selective channel environments. To address this limitation, we propose a symbolblank interval (SBI) frame structure that periodically inserts chirp-only symbols, in which data tones are nulled and only the chirp signal remains. The communication receiver leverages these chirp-only symbols to obtain unbiased channel estimates, while the sensing receiver uses them for interference-free range-Doppler (RD) processing. Simulation results demonstrate that the SBI approach reduces both channel estimation error and bit-error rates compared to conventional SP estimation methods. In addition, the proposed method improves the signal-tointerference-plus-noise ratio on the RD map from 9.54 dB to 18.06 dB, corresponding to an 8.52 dB enhancement. Furthermore, the SBI scheme reduces computational complexity in proportion to the SBI interval length. These results highlight the SBI structure as an effective solution for enhancing both channel estimation and sensing performance in integrated OFDM-FMCW-based JCS systems.

Index Terms—channel estimation, frequency-modulated continuous waveform (FMCW), joint communication and sensing (JCS), orthogonal frequency-division multiplexing (OFDM).

### I. Introduction

Joint communication and sensing (JCS), which performs both sensing and communication functions using a single waveform, has emerged as a key technology for sixth-generation wireless communication systems [1]–[4]. Consequently, the design of waveforms that can efficiently support both communication and sensing functions has become a central task in physical-layer research [5], [6]. Among the various candidates, a waveform that integrates orthogonal frequency-division multiplexing (OFDM) with frequency-modulated continuous waveforms (FMCW) has garnered significant attention [7]. This approach maintains the established advantages of OFDM for communication, such as high spectral efficiency and robustness against multipath fading, while simultaneously enabling low-complexity radar sensing operations [8], [9].

Recent research has demonstrated that the diagonal elements of the inverse discrete Fourier transform (IDFT) matrix can generate chirp-like signals with quadratic phase characteristics [10]. This mathematical property provides a foundation for integration of FMCW chirp signals within the conventional OFDM framework. However, a key challenge arising from this structure is the mutual interference between the communication data and the chirp signal. The FMCW chirp signals can distort the demodulation of communication data, while the communication data symbols can degrade the performance of radar sensing. This interference thus creates a fundamental trade-off between communication reliability and sensing accuracy.

To address this interference, the superimposed-pilot (SP) estimation method has been widely adopted in OFDM-FMCW waveforms, where the FMCW chirp signal serves as an embedded pilot for channel estimation [11]. When the received signal is divided by the known FMCW chirp, the resulting estimate contains a bias term caused by the unknown communication data. At the receiver, the data-induced term behaves randomly, and therefore the SP method averages over multiple OFDM symbols to suppress this bias and obtain accurate channel estimates. However, this reliance on statistical averaging becomes a critical limitation in fast time-selective channels, because the method cannot capture the rapid channel changes that occur within the averaging interval. To overcome these limitations, we propose a symbol-blank interval (SBI) frame structure for OFDM-FMCW waveform. The proposed method periodically disables communication data transmission in specific OFDM symbols and transmits only the FMCW chirp signal, enabling unbiased channel estimation without the need for multi-symbol averaging. Communication receivers use these chirp-only symbols to obtain reliable channel estimates and then demodulate the data symbols in the remaining intervals. For the sensing receiver, the same SBI symbols provide clean chirp observations for radar processing that are free from interference caused by communication data. Furthermore, the proposed SBI scheme modifies only the frame configuration and receiver processing, while maintaining compatibility with conventional OFDM-FMCW waveform designs.

In this paper, we evaluate the communication performance through the bit-error rate (BER) and the normalized meansquared error (NMSE) of channel estimate, and sensing performance is measured by the signal-to-interference-plus-noise ratio (SINR) derived from the range-Doppler (RD) map. The remainder of this paper is organized as follows. Section II introduces the OFDM-FMCW system model and receiver processing. The proposed method for channel estimation is presented in Section III, followed by simulation results in Section IV. Finally, we conclude the paper in Section V.

#### II. OFDM-FMCW SYSTEM MODEL

We consider a monostatic JCS system, as shown in Fig. 1. The transceiver transmits and simultaneously receives echo returns for sensing, while an external receiver decodes the communication payload.

## A. Transmit Signal Model

In the OFDM system, the information bits are mapped to complex-valued data symbols. Here,  $x_q[k]$  denotes the data symbol placed on the k-th subcarrier of the q-th time slot. Accordingly, the discrete-time baseband signal is expressed as

$$s_q[n] = \frac{1}{\sqrt{N}} \sum_{k=0}^{N-1} x_q[k] e^{j\frac{2\pi}{N}kn}, \quad n = 0, \dots, N-1. \quad (1)$$

The same expression can also be written in matrix form as

$$\mathbf{s}_q = \mathbf{F}_N^{-1} \mathbf{x}_q. \tag{2}$$

Here,  $\mathbf{F}_N^{-1}$  denotes the N-point unitary IDFT matrix, whose (n,k)-th element is given by

$$[\mathbf{F}_{N}^{-1}]_{n,k} = \frac{1}{\sqrt{N}} e^{j\frac{2\pi}{N}nk}.$$
 (3)

For the diagonal case where k equals n, the IDFT element becomes  $\frac{1}{\sqrt{N}}e^{j\frac{2\pi}{N}n^2}$ , which has a quadratic phase term similar to a discrete-time linear frequency-modulated (LFM) chirp.

A continuous-time chirp is generally expressed as

$$c(t) = e^{j\pi Kt^2}, \quad 0 \le t < T_c,$$
 (4)

where  $T_c$  is the chirp duration, K is the chirp rate given by  $B_c/T_c$ , and  $B_c$  is the chirp bandwidth. In the OFDM system,

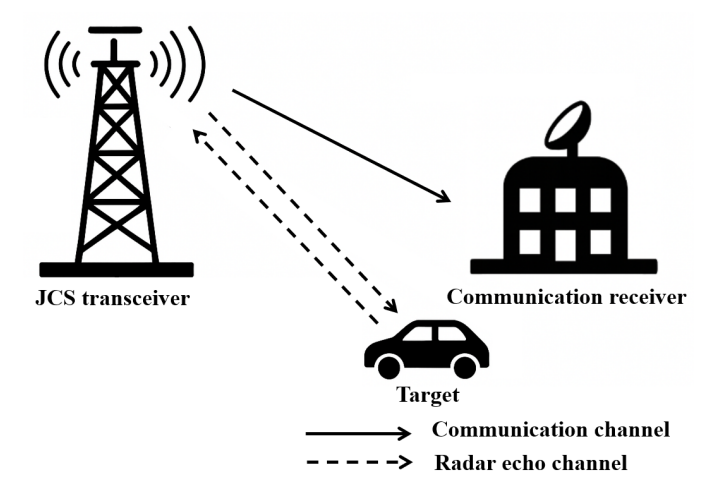


Fig. 1. Monostatic JCS system architecture.

the subcarrier spacing  $\Delta f$  is 1/T, where T is the symbol duration, and the occupied bandwidth B is  $N\Delta f$ , which is equivalent to N/T. If the chirp bandwidth  $B_{\rm c}$  is chosen as B, the chirp rate becomes  $B/T_{\rm c}$ . Sampling at time t defined as nT/N yields

$$c[n] = e^{j\pi \frac{B_c}{T_c} \left(\frac{nT}{N}\right)^2}$$

$$= e^{j\pi \frac{T}{T_c} \frac{n^2}{N}}$$

$$= e^{j\pi \eta \frac{n^2}{N}}, \quad 0 \le n < N,$$
(5)

where  $\eta$  is the normalized chirp rate given by  $T/T_c$ . The similarity between this expression and the quadratic-phase elements of  $\mathbf{F}_N^{-1}$  indicates that an LFM chirp can be directly synthesized within the OFDM modulation framework. To make this structure explicit, we define a diagonal matrix  $\mathbf{C}_N$  whose (n,n)-th element is

$$\left[\mathbf{C}_{N}\right]_{n,n} = \frac{1}{\sqrt{N}} e^{j\pi\eta \frac{n^{2}}{N}}, \quad n = 0, \dots, N - 1,$$
 (6)

where  $\eta$  is set to 2, which makes the diagonal terms identical to those of  $\mathbf{F}_N^{-1}$ . This observation implies that an OFDM symbol can be interpreted as containing a chirp-like component that arises from the IDFT structure. Accordingly, the matrix  $\mathbf{C}_N$  provides a simplified representation of a discrete-time FMCW chirp signal.

Using this representation, the conventional OFDM modulation  $\mathbf{F}_N^{-1}\mathbf{x}_q$  can be decomposed into a chirp component  $\mathbf{C}_N\mathbf{x}_q$  and a residual OFDM component. By separating the chirp component from the OFDM signal and explicitly including an additional chirp, the transmit signal of the q-th symbol becomes

$$\mathbf{s}_q = \left(\mathbf{F}_N^{-1} - \mathbf{C}_N\right) \mathbf{x}_q + P_c \mathbf{C}_N \mathbf{1},\tag{7}$$

where 1 is an all-ones vector of length N, and  $P_c$  denotes the power ratio between the OFDM signal and the chirp signal. The first term represents the OFDM signal with its chirp component removed, whereas the second term denotes a isolated chirp waveform. This structure maintains a clear separation between the data symbols for communication and the chirp signal, and at the same time places both within a single OFDM symbol. Furthermore, since the chirp originates from the diagonal entries of the unitary IDFT matrix, it remains orthogonal to the conventional OFDM subcarriers.

# B. Receiver Processing

The channel observed at the external receiver for communication is modeled as

$$h_c(t) = \sum_{l=1}^{L_c} \sigma_{c,l} \, \delta(t - \tau_{c,l}), \tag{8}$$

where  $L_c$  is the number of channel taps,  $\sigma_{c,l}$  is the complex gain, and  $\tau_{c,l}$  is the delay of the l-th propagation path.

Similarly, the channel observed at the monostatic transceiver for sensing is expressed as

$$h_r(t) = \sum_{l=1}^{L_r} \sigma_{r,l} \, \delta(t - \tau_{r,l}),$$
 (9)

where  $L_r$  is the number of channel taps,  $\sigma_{r,l}$  is the complex gain, and  $\tau_{r,l}$  is the delay of the l-th reflection path. By sampling over the symbol duration, the discrete-time baseband model is obtained as

$$y_i[k] = \sum_{l=0}^{L_i - 1} h_{i,l} \, s[k - \tau_{i,l}] + w_i[k], \qquad i \in \{c, r\}, \quad (10)$$

where  $w_i[k]$  denotes additive white Gaussian noise.

At the communication receiver, the cyclic prefix (CP) is removed and an N-point discrete Fourier transform is applied to the received signal. The resulting frequency-domain observation can be written as

$$\mathbf{Y}_{q} = \mathbf{F}_{N} \mathbf{H}_{q} \left( (\mathbf{F}_{N}^{-1} - \mathbf{C}_{N}) \mathbf{x}_{q} + P_{c} \mathbf{C}_{N} \mathbf{1} + \mathbf{w} \right)$$

$$= \underbrace{\mathbf{F}_{N} \mathbf{H}_{q} \mathbf{F}_{N}^{-1} \mathbf{x}_{q}}_{\mathcal{S}} + \underbrace{P_{c} \mathbf{F}_{N} \mathbf{H}_{q} \mathbf{C}_{N} \mathbf{1}}_{\mathcal{P}} + \mathbf{W}_{add}, \tag{11}$$

where  $\mathcal{S}$  denotes the communication term. The chirp-induced term  $\mathcal{P}$  is known a priori and can therefore be used as a pilot. Finally,  $\mathbf{W}_{add}$  represents additional noise, including residual cross terms, which arise from the superposition of data and chirp components and remain after normalization.

Because the communication and pilot terms are superimposed, channel estimation is performed using a superimposed-pilot (SP) least-squares (LS) estimator. In this approach, the received vector is divided element-wise by the known pilot. The channel estimate is obtained as

$$\widehat{\mathbf{H}}_{q} = \mathbf{Y}_{q} \oslash (P_{c} \mathbf{F}_{N} \mathbf{C}_{N} \mathbf{1}) 
= \mathbf{H}_{q} \left( \mathbf{1} + \frac{\mathbf{x}_{q}}{P_{c} \mathbf{C}_{N} \mathbf{1}} \right) + \mathbf{W}'_{\text{add}},$$
(12)

where  $\oslash$  denotes element-wise division and  $\mathbf{W}'_{\text{add}}$  is the effective noise after normalization. For a time-invariant channel, the data-induced term has zero mean because of the constellation property. The residual bias can be reduced by averaging the channel estimates across Q symbols as

$$\widehat{\mathbf{H}} = \frac{1}{Q} \sum_{q=1}^{Q} \widehat{\mathbf{H}}_{q}.$$
 (13)

Using this averaged channel estimate, the chirp pilot is removed from the received signal and one-tap equalization is applied. The equalized data symbol is obtained as

$$\widehat{\mathbf{x}}_{q} = \left(\mathbf{Y}_{q} - P_{c} \,\widehat{\mathbf{H}}_{q} \,\mathbf{C}_{N} \mathbf{1}\right) \otimes \widehat{\mathbf{H}}$$

$$= \mathbf{x}_{q} + \mathbf{W}', \tag{14}$$

where W' denotes the residual noise remaining after pilot cancellation and equalization.

At the sensing receiver, the received signal is first multiplied by the conjugate reference chirp. As given in (7), the superimposed transmit waveform s(t) consists of  $s_{\text{comm}}(t)$ 

and  $P_c c(t)$ , where  $s_{\text{comm}}(t)$  denotes the communication part. The received signal is then expressed as

$$r(t) = \sum_{r=1}^{R} \alpha_r \, s(t - \tau_r) \, e^{j2\pi f_{d,r}(t - \tau_r)} + w(t), \qquad (15)$$

where  $\alpha_r$ ,  $\tau_r$ , and  $f_{d,r}$  denote the complex amplitude, round-trip delay, and Doppler shift of the r-th target, respectively, and w(t) represents additive white Gaussian noise. The received signal is dechirped by multiplying it with the conjugate reference chirp  $c^*(t)$ , which yields

$$\tilde{r}(t) \triangleq r(t)c^{*}(t)$$

$$= \sum_{r=1}^{R} \alpha_{r} P_{c} c(t - \tau_{r}) e^{j2\pi f_{d,r}(t - \tau_{r})} c^{*}(t)$$

$$+ \sum_{r=1}^{R} \alpha_{r} s_{\text{comm}}(t - \tau_{r}) e^{j2\pi f_{d,r}(t - \tau_{r})} c^{*}(t) + \tilde{w}(t),$$
(16)

where  $\tilde{w}(t)$  equals to  $w(t)c^*(t)$ . The first term corresponds to the desired FMCW dechirped response, and the second term represents interference from the communication signal. Adjusting the chirp power ratio  $P_c$  can partially mitigate this interference. However, increasing  $P_c$  also lowers the relative power of the data signal and may degrade demodulation performance. The beat frequency  $f_{b,r}$ , approximated by  $K\tau_r$ , is obtained from a fast Fourier transform (FFT) along the fast-time axis, while the Doppler shift  $f_{d,r}$  is estimated from an FFT along the slow-time axis.

From a radar perspective, the presence of the cyclic prefix (CP) breaks the chirp continuity at the boundaries of consecutive OFDM symbols, which complicates dechirping. Because the CP repeats the last samples of each symbol, a phase discontinuity arises at symbol boundaries, unlike in a conventional FMCW waveform. To overcome this issue, we introduce a frequency-domain linear phase corresponding to a cumulative time shift of  $iL_{\rm cp}$  samples, thereby restoring chirp continuity across N-sample blocks. This can be expressed as

$$c^{(i)}[n] \triangleq \mathbf{F}_N^{-1} \left( \operatorname{diag} \left( e^{j\frac{2\pi}{N}(iL_{\text{cp}})k} \right) \mathbf{F}_N \mathbf{C}_N \mathbf{1} \right)$$

$$= c[n - iL_{\text{cp}}],$$
(17)

where  $\operatorname{diag}(\cdot)$  denotes a diagonal matrix formed from a vector argument. This compensation preserves the primary role of the CP in communication. It ensures channel circularity and suppresses inter-symbol interference, and it also maintains chirp continuity for sensing. As a result, direct dechirping is enabled without discarding the CP, and the radar receiver design becomes simpler.

# III. PROPOSED SBI-AIDED CHANNEL ESTIMATION AND SENSING

To overcome the limitations of SP estimation, we propose a SBI structure. In the proposed approach, specific OFDM symbols are allocated for sensing, where the data tones are nulled and only the chirp signal is exploited for sensing. An SBI is inserted periodically with an interval of M symbols. This design enables interference-free channel estimation within the same frame, because the chirp is observed without data interference. An example with a pilot interval M of 4 is shown in Fig. 2. These SBIs thus serve as pilot symbols for both channel estimation and sensing. Let  $\mathcal{Q}_0$  denote the index set of SBI symbols, and let  $\mathcal{Q}_1$  denote its complement. For  $q \in \mathcal{Q}_0$ , we set  $\mathbf{x}_q$  to zero. In this case, the received signal simplifies to

$$\mathbf{Y}_{q} = P_{c}\mathbf{F}_{N}\mathbf{H}_{q}\mathbf{C}_{N}\mathbf{1} + \mathbf{W}_{q}, \qquad q \in \mathcal{Q}_{0}. \tag{18}$$

From this expression, we obtain a channel estimate that is free from data interference.

$$\widehat{\mathbf{H}}_{SBI} \triangleq \mathbf{Y}_q \oslash \left( P_c \mathbf{F}_N \mathbf{C}_N \mathbf{1} \right) 
= \mathbf{H}_q + \mathbf{W}_{eff},$$
(19)

where  $\mathbf{W}_{\mathrm{eff}}$  denotes the effective noise term after normalization. Compared with the SP expressions in (11) and (12), the SBI scheme is much simpler. In the SP estimator, the pilot and data symbols are superimposed, so that residual interference from data remains even after normalization. In contrast, the SBI symbols contain no data, and thus the channel can be directly estimated from the known chirp component. The channel is first estimated at the SBI positions, and the values at the intermediate symbols are obtained by linear interpolation [12]. Specifically, when a data symbol  $q \in \mathcal{Q}_1$  lies between two adjacent SBIs indexed by  $q_m$  and  $q_{m+1}$ , we introduce the parameter  $\alpha$ , defined as the ratio  $(q-q_m)/(q_{m+1}-q_m)$ . The channel estimate is then interpolated across OFDM symbols as

$$\widehat{H}[k,q] = (1-\alpha)\,\widehat{H}_{\mathrm{SBI}}[k,\,q_m] + \alpha\,\widehat{H}_{\mathrm{SBI}}[k,\,q_{m+1}]. \tag{20}$$

Here,  $\hat{H}_{SBI}$  denotes the channel estimates obtained at the SBI symbols. The SBI-based approach requires only a few modifications to the frame scheduling and receiver processing, while the OFDM–FMCW signal structure itself remains unchanged. Unlike the SP method, the channel estimates from  $\mathcal{Q}_0$  are unaffected by data interference and therefore remain accurate

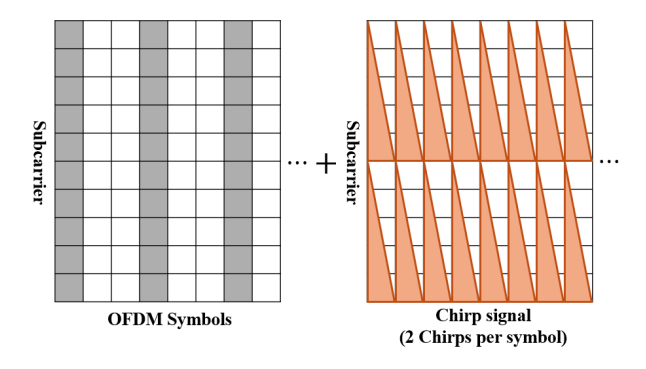


Fig. 2. Proposed frame structure with a pilot interval M of 4: gray symbols represent SBIs with nulled data tones and chirp-only transmission, while white symbols carry OFDM data combined with the chirp signal.

even under rapid channel variations. The pilot overhead is given by

$$\rho = \frac{|Q_0|}{|Q_0| + |Q_1|},\tag{21}$$

which simplifies to 1/M when an SBI is inserted every M symbols. The interval M is chosen such that the SBI spacing lies within the channel coherence time. This ensures reliable channel estimation while keeping the loss in transmission rate small.

The sensing receiver also benefits from the SBI structure. When  $q \in \mathcal{Q}_0$ , the data vector  $\mathbf{x}_q$  becomes zero, and the received symbol therefore contains only the chirp signal. The corresponding dechirped output is

$$r_{\text{SBI}}(t) = \sum_{r=1}^{R} \alpha_r P_c c(t - \tau_r) e^{j2\pi f_{d,r}(t - \tau_r)} c^*(t) + \tilde{w}(t),$$
(22)

which is equivalent to (16) but without the interference from communication data. This offers clean inputs for RD processing and improves the SINR compared with conventional SP operation.

In the SBI scheme, however, only the SBI symbols are available for sensing. As a result, the number of OFDM symbols usable for Doppler processing decreases in proportion to the pilot ratio 1/M. This effectively down-samples the slow-time sequence by a factor of M, reducing the maximum unambiguous Doppler range by 1/M [13]. The Doppler resolution, on the other hand, remains unchanged because the overall frame duration is preserved.

## IV. PERFORMANCE EVALUATION

We evaluate the proposed SBI-based channel estimation and sensing scheme in terms of both communication and sensing performance. For communication, the metrics are the BER after one-tap equalization and the NMSE of the channel estimates. For sensing, the quality of the RD map is measured by the SINR, and RD maps are plotted to illustrate the effect of SBI gating on target detection. The simulation uses a carrier frequency  $f_c$  of 77 GHz and a bandwidth B of 200 MHz. The simulation employs a number of subcarriers N of 1024 and a number of OFDM symbols per frame Q of 100, with an SBI schedule of 1:4. The CP ratio is set to  $L_{\rm cp}/N$  of 1/4, and the chirp power ratio is  $P_c$  of 1.

We first compare uncoded BER versus SNR. Fig. 3 shows that the proposed SBI method consistently outperforms the SP-LS estimator over the 5–30 dB range. For the same BER, the proposed SBI method requires a lower SNR than the SP-LS estimator. This BER gain directly follows from the more accurate channel estimates obtained by SBI, which prevent error propagation in equalization. The channel estimation accuracy is quantified using the NMSE, which is expressed

NMSE = 
$$\frac{\sum_{q=1}^{Q} \sum_{k=1}^{N} \left| H[k, q] - \widehat{H}[k, q] \right|^{2}}{\sum_{q=1}^{Q} \sum_{k=1}^{N} \left| H[k, q] \right|^{2}}.$$
 (23)

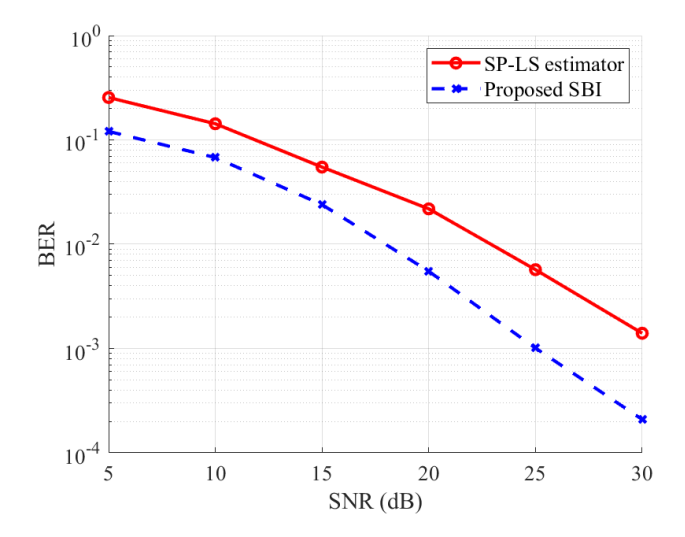


Fig. 3. Comparison of BER versus SNR under Rayleigh fading for the SP-LS estimator and the proposed SBI method.

Table I lists the average NMSE over the SNR range of 5-30 dB. The proposed method achieves an NMSE of  $-17.15\,\mathrm{dB}$  compared with  $-11.28\,\mathrm{dB}$  for the SP-LS estimator, corresponding to an improvement of about 6 dB in estimation accuracy. This gain is particularly important in fast time-selective fading channels. In such environments, interpolation between SBIs can effectively track intra-frame channel variations, as long as the interval M remains within the channel coherence time. In contrast, SP-LS requires multi-symbol averaging to suppress the data term. This averaging smooths out rapid channel variations and leaves residual bias, which degrades equalization performance and increases the BER.

For sensing evaluation, we adopt the SINR as the performance metric. SINR captures the residual data-induced interference that arises when chirps are superimposed on data symbols. Let  $P_{\rm sig}$  denote the power of the target bin, and let  $P_{\rm IN}$  denote the average interference-plus-noise power within a surrounding region that excludes a guard interval around the target. The SINR is given by

$$SINR = 10 \log_{10} \left( \frac{P_{\text{sig}}}{P_{\text{IN}}} \right). \tag{24}$$

Table I also includes the average SINR over 5–30 dB. The proposed method achieves  $18.06\,\mathrm{dB}$  compared with  $9.54\,\mathrm{dB}$  for the SP-LS estimator, resulting in an average gain of about  $8.52\,\mathrm{dB}$ . This improvement arises because communication-induced interference is eliminated when RD maps are formed from SBI symbols. On the other hand, only a fraction  $\rho$  of the OFDM symbols is available for RD processing. Consequently,

TABLE I AVERAGE NMSE AND SINR OVER  $5-30\,\mathrm{DB}$  SNR

	SP-LS estimator	Proposed SBI
NMSE (dB)	-11.28	-17.15
SINR (dB)	9.54	18.06

the maximum unambiguous velocity is reduced by the same factor  $\rho$ .

Fig. 4 illustrates RD maps with two targets at  $(50\,\mathrm{m}, -20\,\mathrm{m/s})$  and  $(200\,\mathrm{m}, 20\,\mathrm{m/s})$ . With the SP-LS estimator, residual communication interference raises the noise floor and produces clutter around the targets. In contrast, the proposed method produces a significantly cleaner RD map with substantially reduced background interference. The suppression of clutter observed in Fig. 4 is quantitatively confirmed by the SINR improvement summarized in Table I.

In addition to performance metrics, we also compare the computational complexity of the two approaches, as summarized in Table II. The SP-LS estimator requires normalization for all Q symbols, which results in O(NQ) complex divisions followed by averaging across symbols. In contrast, the proposed method performs normalization only at the chirp-only

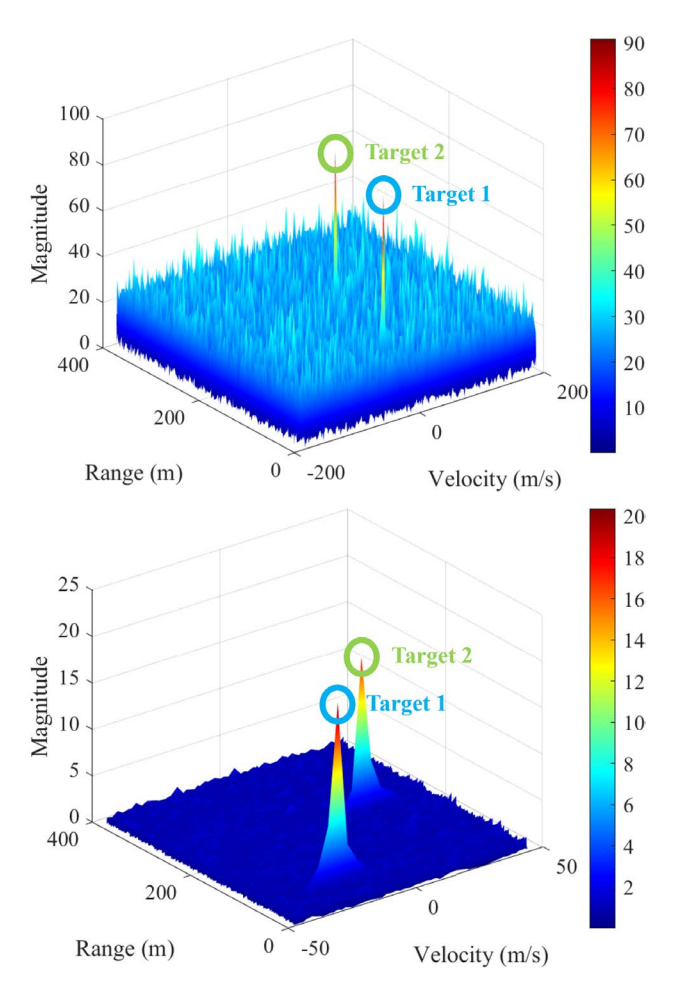


Fig. 4. RD maps at  $P_c = 1$  with two targets, obtained using the SP-LS estimator (top) and SBI-based processing (bottom).

	SP-LS estimator	Proposed SBI
Channel estimation	O(NQ)	O(NQ/M)
Doppler FFT	$O(Q \log Q)$	$O((Q/M)\log(Q/M))$

symbols, reducing the division cost to O(NQ/M). The channels of the remaining symbols are recovered through linear interpolation. This operation involves only multiplications and additions and is therefore much less demanding than divisions. On the sensing side, the Doppler FFT length decreases from Q to Q/M, which lowers the cost from  $O(Q\log Q)$  to  $O((Q/M)\log(Q/M))$ . Consequently, the proposed method achieves an M-fold reduction in the dominant computational complexity.

### V. CONCLUSION

In this paper, we proposed an SBI scheme for OFDM-FMCW waveforms to address the challenges of channel estimation and mutual interference in JCS systems. The proposed method periodically disables communication data transmission in specific OFDM symbols, which provides unbiased channel estimates for communication receivers and clean observations for sensing receivers. Simulation results demonstrate that the SBI approach achieves superior performance compared to conventional SP methods. In terms of communication performance, the proposed SBI method achieved an NMSE of  $-17.15 \, dB$  compared with  $-11.28 \, dB$  for the SP method, and it required a lower SNR to reach the same BER. For sensing performance, the proposed method yielded an 8.5 dB enhancement in the SINR on the RD map, increasing from 9.54 dB to 18.06 dB. Beyond these performance metrics, the SBI scheme offers a significant practical advantage by reducing computational complexity in proportion to the SBI interval.

### ACKNOWLEDGMENT

This work was supported by the National Research Foundation of Korea (NRF) grant funded by the Korea government (MSIT) (No. RS-2024-00405510).

# REFERENCES

- [1] J. A. Zhang, A. Cantoni, X. Huang, Y. J. Guo, and R. W. Heath, "Enabling joint communication and radar sensing in mobile networks: A survey," *IEEE Communications Surveys & Tutorials*, vol. 22, no. 1, pp. 61–96, October 2020.
- [2] X. Cheng, D. Duan, S. Gao, and L. Yang, "Integrated sensing and communications (ISAC) for vehicular communication networks (VCN)," *IEEE Internet of Things Journal*, vol. 9, no. 23, pp. 23441–23451, December 2022.
- [3] X. Fang, W. Feng, Y. Chen, N. Ge, and Y. Zhang, "Joint communication and sensing toward 6G: Models and potential of using MIMO," *IEEE Internet of Things Journal*, vol. 10, no. 5, pp. 4093–4116, March 2023.
- [4] Z. Wei et al., "Integrated sensing and communication signals toward 5G-A and 6G: A survey," *IEEE Internet of Things Journal*, vol. 10, no. 13, pp. 11068–11092, July 2023.
- [5] M. M. Sahin, I. E. Gurol, E. Arslan, E. Basar, and H. Arslan, "OFDM-IM for joint communication and radar-sensing: A promising waveform for dual functionality," *Frontiers in Communications and Networks*, vol. 2, pp. 1–9, August 2021.
- [6] D. Ma, N. Shlezinger, T. Huang, Y. Liu, and Y. C. Eldar, "FRaC: FMCW-based joint radar-communications system via index modulation," *IEEE Journal of Selected Topics in Signal Processing*, vol. 15, no. 6, pp. 1348–1364, October 2021.
- [7] Y. Ma, Z. Yuan, G. Yu, S. Xia, and L. Hu, "A spectrum efficient waveform integrating OFDM and FMCW for joint communications and sensing," *IEEE International Conference on Communications Work-shops*, Seoul, South Korea, May 2022, pp. 475–479.

- [8] H. K. Boddapati, K. Kumar, A. K. R. Chavva, and M. S. Khan, "Joint communication and sensing for MIMO systems with overlapped OFDM and FMCW," *IEEE Vehicular Technology Conference (VTC2023-Fall)*, Hong Kong, China, September 2023, pp. 1613–1618.
- [9] J. Liu, W. Feng, T. Su, J. Chen, and S. Xue, "Millimeter-wave OFDM-FMCW radar-communication integration system design," *Remote Sensing*, vol. 17, no. 6, pp. 1–22, March 2025.
- [10] A. Bouziane, S. E. Zegrar, and H. Arslan, "A novel OFDM-FMCW waveform for low-complexity joint sensing and communication," *IEEE Wireless Communications Letters*, vol. 14, no. 2, pp. 425–432, February 2025.
- [11] P. Hoeher and F. Tufvesson, "Channel estimation with superimposed pilot sequence," *IEEE Global Telecommunications Conference*, Rio de Janeiro, Brazil, December 1999, vol. 4, pp. 2162–2166.
- [12] X. Dong, W.-S. Lu, and A. C. K. Soong, "Linear interpolation in pilot symbol assisted channel estimation for OFDM," *IEEE Transactions on Wireless Communications*, vol. 6, no. 5, pp. 1910–1920, May 2007.
- [13] S. Kwak, D. Jeon, and S. Lee, "Adjusting detectable velocity range in FMCW radar systems through selective sampling," *IEEE Journal of Selected Areas in Sensors*, vol. 1, pp. 249–260, October 2024.